




A comparative study on structural, morphological and photocatalytic properties of anodically grown ZnO nanowires under varying parameters

Erdem Tevfik Ozdemir¹, Ugur Kartal^{2,*} , Tuncay Dikici^{3,4}, Mustafa Erol^{4,5}, and Metin Yurddaskal⁵

¹The Graduate School of Natural and Sciences, Dokuz Eylul University, Izmir, Turkey

²Department of Materials Science and Engineering, Izmir Institute of Technology, Izmir, Turkey

³Torbali Vocational School, Dokuz Eylul University, Izmir, Turkey

⁴Center for Fabrication and Application of Electronic Materials, Dokuz Eylul University, Izmir, Turkey

⁵Department of Metallurgical and Materials Engineering, Dokuz Eylul University, Izmir, Turkey

Received: 24 May 2021

Accepted: 24 September 2021

Published online:

29 September 2021

© The Author(s), under exclusive licence to Springer Science+Business Media, LLC, part of Springer Nature 2021

ABSTRACT

In this study, zinc oxide (ZnO) nanowires (NWs) were successfully produced on Zn plates through electrochemical anodization in potassium bicarbonate aqueous electrolytes with different production parameters in two groups as applied voltage and anodization time. Subsequently, the ZnO NWs were annealed at 300 °C for 1 h in air atmosphere to increase crystallinity and remove organic residues. Structural and morphological properties were determined through X-ray diffraction (XRD) and scanning electron microscopy (SEM) analysis. The effect of anodization parameters on the structure of ZnO NWs and thus their photocatalytic activities were evaluated in detail by UV spectrophotometer. The results pointed out that, the most effective nanostructure on the photocatalytic degradation of methylene blue was obtained in the sample that was anodized for 30 min under 30 V at room temperature with a degradation efficiency of 90.6% after 11 h. This result shows that the NW-structured ZnO materials are promising to be used as effective photocatalysts in the removal of organic pollutants by solar energy and their conversion to green compounds.

1 Introduction

Semiconductors are environmentally friendly materials that have a wide range of daily applications and do not pose major environmental risks. The metal oxide semiconductors (ZnO, TiO₂, Fe₂O₃, CuO, NiO,

etc.) have favorable properties that desired in a variety of applications [1]. One of these applications is photocatalysis and some semiconductors, such as TiO₂ and ZnO, are heavily utilized for the degradation of environmental contaminants [2–5]. Photocatalysis, also known as photo-assisted catalysis, has

Address correspondence to E-mail: ugurkartal@iyte.edu.tr

processes similar to photosynthesis [3]. When photons with energies greater than the bandgap energy of the photocatalyst are absorbed, at least two reactions occur simultaneously and carbon dioxide and water come out of degradation of various organic compounds [6]. After publication of Fujishima and Honda on photocatalytic water splitting via TiO_2 in 1972, studies on TiO_2 as a photocatalyst have increased considerably [7]. Although the TiO_2 photocatalyst is widely used, ZnO is a feasible alternative to be photocatalyst because of its bandgap energy and its relatively lower cost of production [8, 9].

ZnO is a n-type semiconductor that has been receiving a great attention in the last decade [5]. ZnO, with a wide bandgap (3.37 eV) and large exciton binding energy (60 meV) [10–13], has found a wide range of possible applications in photocatalysis [14], photovoltaics [15], light-emitting diodes [16], sensing [17] and many others [18].

One-dimensional (1D) nanostructures have been studied affluently due to their high charge transport efficiency and surface to volume ratio [19]. ZnO nanowires (NWs) is the most engaging nanostructures of ZnO. Up to now, several different synthesis methods to fabricate ZnO NWs have been used in the literature, e.g., hydrothermal methods [20], chemical vapor deposition [21], template-directed methods [22], sol-gel [11], molecular beam epitaxy [23], atomic layer deposition [24], pulsed laser deposition [25], or direct precipitation [26]. Nonetheless, most of these methods required long reaction times, expensive experimental setups and complicated procedures.

Apart from the methods mentioned above, electrochemical anodization is an efficient, highly controllable, fast, and cost-effective method to produce the ZnO NWs. Furthermore, this method has the advantage of growing nanostructures in situ without the requirement for an additional substrate (FTO, Si, etc.) [12, 27, 28]. Because of these intriguing properties, this method has gained much attention after the demonstration of the two-step approach by Masuda and Fukuda in 1995 [29]. The oxidizing of a surface of an anode metal is provided through electrochemical anodization method, in a specific electrolyte under a specific voltage at room temperature, resulting in the formation of various nanostructured materials, e.g., nanoporous-like structures, nanoflakes, nanoflowers, nanoneedles, and NWs [1, 30, 31].

The conditions applied during anodization, including electrolyte concentration, applied potential,

temperature and duration of the process, have a profound effect on the physical and chemical properties of the NWs [12]. Hu et al. fabricated ultralong ZnO NW arrays by anodizing Zn foil at room temperature in 5–50 mM KHCO_3 aqueous solution [10]. Miles et al. reported that they have successfully fabricated hierarchical ZnO NWs with a high aspect ratio via anodization of Zn foil by controlling various parameters such as the types of bicarbonate electrolytes, experimental temperature, electrolyte concentration. [30]. It is obvious that bicarbonate solutions are very popular electrolytes for anodizing Zn to obtain ZnO NWs, as they allow a rapid formation under suitable conditions [32]. Some authors have studied the utilizing of ZnO nanowires produced by anodizing in applications such as photoelectrochemical water splitting [27, 33] and solar cells [34]. Although such aforementioned studies dealing with the parametric study of the process parameters on the production of ZnO NWs are available in the literature, to the best of our knowledge, few studies are evaluating these effects on the photocatalytic activities of the ZnO NWs, and thus it needs further investigation for better understanding structure–activity correlation.

Herein, we reported the study on electrochemical anodization of zinc in aqueous electrolytes, with the main focus being on the effects of anodization voltage and anodization time on the photocatalytic performances of the nanostructured ZnO. The phase structures, surface morphologies and photocatalytic activities of ZnO NWs were examined in detail.

2 Experimental studies

2.1 Materials

Zn plate (99.9%, thickness 1 mm) was supplied by BByes Store. Potassium bicarbonate (KHCO_3 , 99.7%), absolute ethanol ($\text{C}_2\text{H}_5\text{OH}$, $\geq 99.9\%$) and isopropyl alcohol ($\text{C}_3\text{H}_8\text{O}$, 99.5%) were supplied from Merck and used as purchased.

2.2 Synthesis of ZnO NWs

Anodization samples of $25 \times 25 \text{ mm}^2$ dimensions were cut from Zn plate. Subsequently, the Zn substrates were washed with ethanol and distilled water in an ultrasonic cleaner (Everest CleanEx-2511) for

15 min, respectively. Cleaned substrates were dried at room temperature in the air atmosphere. Applied anodization parameters to the Zn substrates were categorized and listed in Table 1. Anodization was performed under different voltages (10–40 V) and times (10–120 min) for investigating the anodization parameters on the structure of produced ZnO NWs which has a certain effect on the photocatalytic activity [35]. For anodization process, a two-electrode electrochemical cell setup (Fig. 1) containing Zn plate as a working electrode, stainless steel plate as a counter electrode and aqueous solution of KHCO_3 (50 mM) as an electrolyte was used. The distance between two electrodes was kept at 10 cm through anodization process. The anodized samples were rinsed with distilled water and isopropyl alcohol to remove remaining electrolyte, respectively. Afterward, the samples were put in a drying oven (Binder ED53) at 80 °C for 60 min. Finally, the as-anodized samples were annealed at a temperature of 300 °C for 1 h at a heating rate of 2 °C min^{-1} and stored in a desiccator before characterization.

2.3 Materials characterization

In order to elucidate the phase structure, as-anodized and annealed samples were examined by an X-ray diffractometer (XRD, Thermo Scientific ARL X'TRA) with a $\text{Cu-K}\alpha$ (1.54185 Å) irradiation in the range of $2\theta = 10\text{--}90^\circ$ at a scan rate of 2° min^{-1} . The surface morphology and nanostructure of the samples were observed by a scanning electron microscope (SEM, Carl Zeiss 300VP).

Table 1 Anodization parameters of ZnO NWs

Group	Sample Code	Voltage (V)	Time (min)
Group 1	S1	10	30
	S2	20	30
	S3	30	30
	S4	40	30
Group 2	S5	10	10
	S6	10	20
	S7	10	60
	S8	10	120

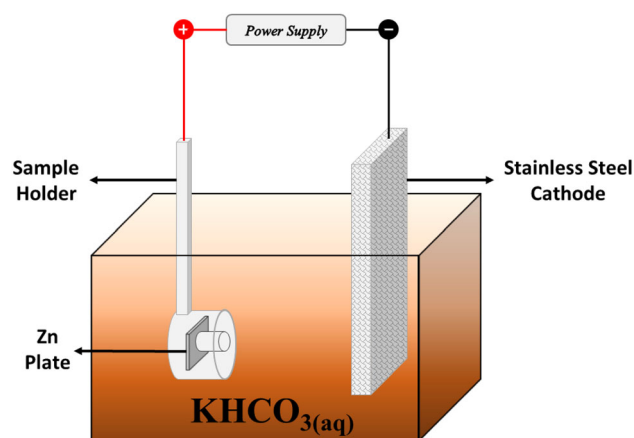


Fig. 1 Schematic of electrochemical cell setup

2.4 Photocatalytic measurements

The photocatalytic activities of the samples were scrutinized using 10^{-5} M of methylene blue (MB) solution under 300 W Osram Ultra-Vitalux E27 (4.53% UVA, 1% UVB, 94.47% Vis) light source at room temperature. In order to compare catalyst-free degradation of MB under irradiation a reference solution was also prepared. The photocatalysts were immersed into 30 mL of MB aqueous solution in beakers and placed under the light source with a distance approximately 20 cm. In order to determine the absorbencies, 3 ml of the MB solution from each beaker was taken out after UV light exposure at 2-h intervals starting from 1 h. The absorption measurements of the MB solution were performed at the wavelength from 400 to 800 nm and confirmed by monitoring the decreasing of absorbance at 664 nm, which is the characteristic peak of MB [36], by a UV spectrophotometer (Shimadzu UV 1240 spectrophotometer). Within the scope of Lambert Beer Law, the absorbance values were converted to concentration values [37]. Their photocatalytic degradation efficiency was defined as $[(C_0 - C)/C_0] \times 100$ (C_0 ; initial concentration, C ; final concentration). For the final step of characterization, photocatalytic reaction kinetics on MB degradation were calculated for all samples using the catalysts.

3 Results and discussion

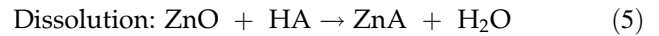
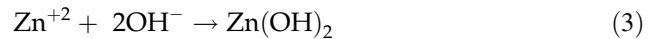
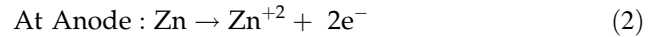
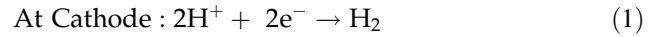
3.1 Structural analysis

The structures of the as-anodized and annealed ZnO NWs were analyzed via the XRD technique. The XRD patterns of ZnO NWs which produced at different voltages and anodization time by electrochemical anodization method are shown in Fig. 2, b for sample groups 1 and 2, respectively. Figure 2 depicts the diffraction peaks with 2θ values 31.69, 34.28, 36.26, 56.53, and 62.66 which correspond to the ZnO lattice planes with Miller Indices (100), (002), (101), (110), and (103) (ICDD 00–036-1451), respectively. Nevertheless, there are few diffraction peaks with 2θ values 36.26, 38.71, 43.13, 54.17, and 69.93 which correspond to the Zn substrate lattice planes with Miller Indices (002), (100), (101), (102), and (103) (ICDD 03–065-5973), respectively [1]. As shown in Fig. 2a, b, the peak intensities of the ZnO structures were increased with increasing applied voltage and anodization time. Thus, the amount of ZnO structure in the produced samples was increased. The structural data of

the samples were found to be similar to the literature [1, 10, 34].

3.2 Morphological analysis

Upon the initial voltage is applied, discrete and small pits are formed by electrochemical etching and Zn^{+2} ions emerge from the zinc plate. The main chemical reactions can be represented as follows:



where “A” refers to the HCO_3^- ions from the bicarbonate solution.

Due to the increase in Zn^{+2} ion density, nanoflower structures begin to form around the pits and as a result of the continuation of the reactions, the growth

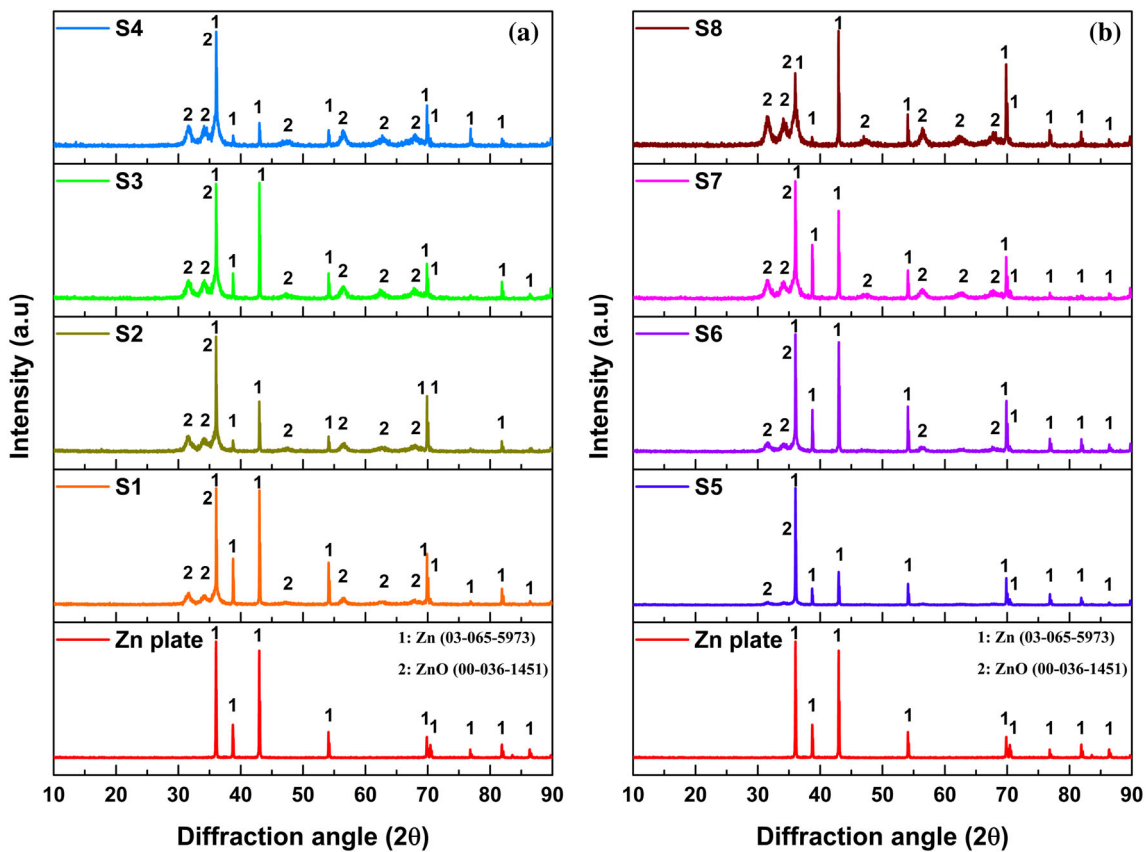


Fig. 2 XRD patterns of the samples a Group 1, b Group 2

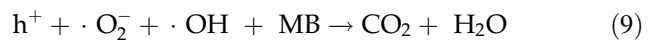
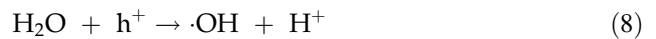
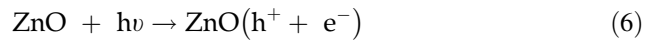
of the structures occurs and ZnO NWs are observed all over the plate surface.

Figure 3 shows the surface images of the ZnO NWs were obtained at different voltages such as 10, 20, 30 and 40 V. As seen in Fig. 3a, the formation of aligned nanowires structures started at an initial point of growth. When Fig. 3b, c are examined, well-ordered ZnO NW structures were seen that completely covering the surface of the Zn plate with the effect of increasing voltage. ZnO NWs have become thinner and denser structures with their diameters decreasing from 217 to 64 nm through increasing anodizing voltage. When the applied voltage was increased to 40 V, there were linked and interpenetrated structures due to the length of the NWs as seen in Fig. 3d. Furthermore, micro cracks were observed on the surface due to oxygen evolution during anodization at high voltage as shown in Fig. 3e with green line dashes. Since the anodization process is accelerated under high voltages, more O atoms are expected to be produced at the zinc/solution interface, and O₂ gas is supposed to release rapidly. Therefore, vigorous oxygen evolution may cause micro cracks and discontinuities on the Zn plate surface. That is in line with that reported by Hu et al. [10]. Figure 4 indicates the effects of anodizing time on the morphology of ZnO NWs. The results show that as the anodizing time increases, the diameters of the ZnO NWs decreased from 263 to 112 nm. Therefore, the NW density (the total number of NWs occupying a unit area of 1 cm²) is increased. The diameters of group 1 and 2 samples are given in Fig. 5. The tangled ZnO NWs structure has emerged after anodization for 60 min. As seen in literature, these results are in good agreement with the previously published studies [19, 30, 32].

3.3 Photocatalytic activity

The charge transfer pathway in the photocatalytic mechanism of the ZnO NWs with different morphological properties can be explained and understood based on Fig. 6. Due to the light excitation to the ZnO NWs, electron–hole pairs occur. In this way, holes (h⁺) form in the valence band, while electrons (e⁻) transfer to the conduction band [38–40]. Thus, with the light irradiation, superoxide radical anions (•O₂⁻) and hydroxyl radicals (•OH) form, respectively [41, 42]. These surface species formed can participate in the photocatalytic degradation process

over the ZnO NWs [26]. In consequence of the photocatalytic degradation, the MB turns into green compounds such as carbon dioxide (CO₂) and water (H₂O) [43, 44]. The reactions that occur during the degradation of MB under UV light source can be listed as follows:



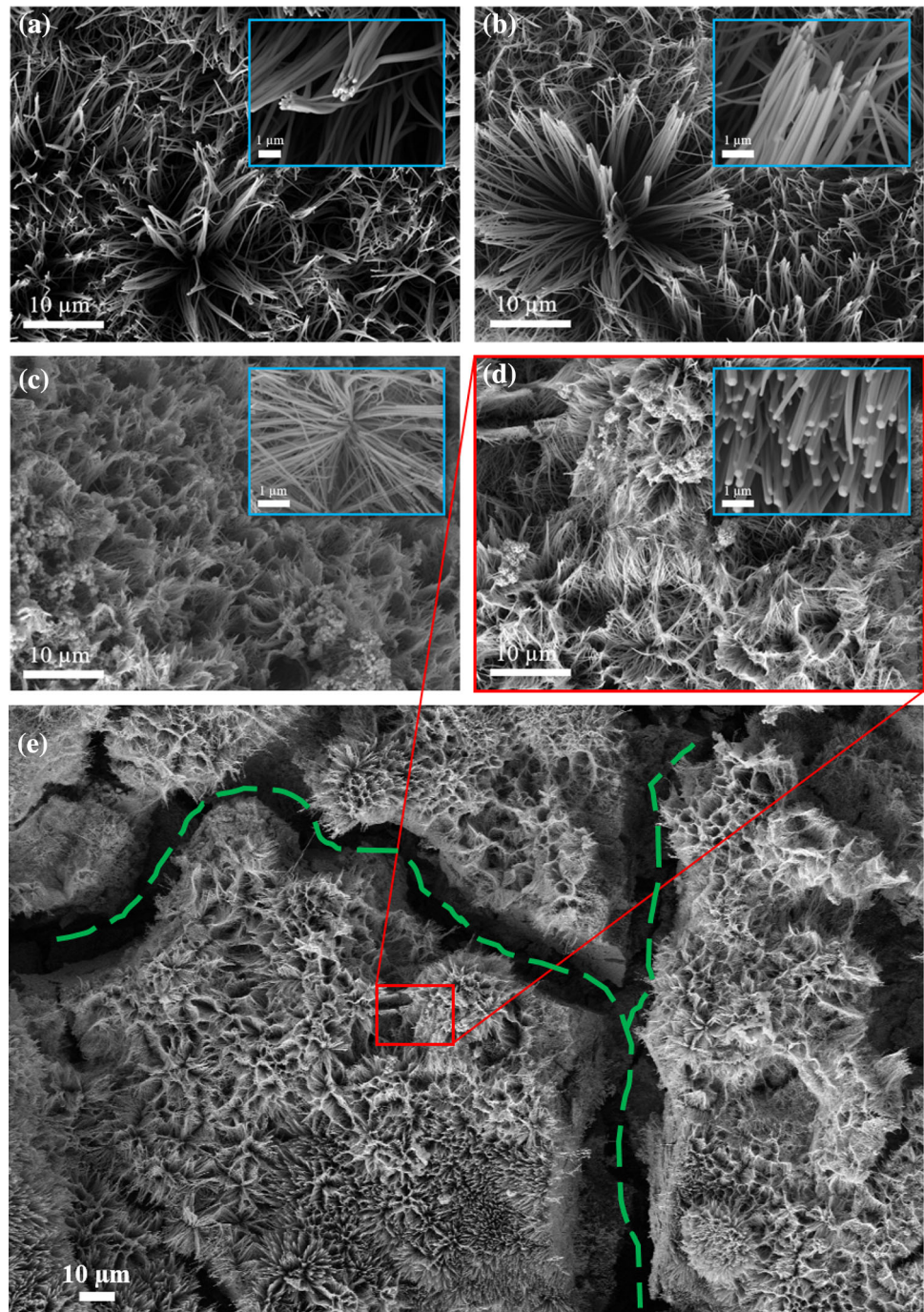
The photocatalytic performances of the samples were obtained by measuring the absorbance data of the samples taken from the degraded MB at certain time intervals. The MB aqueous solution under UV–Vis light irradiation is degraded by photocatalysts thanks to the photocatalytic effect. Figure 7a shows the change in concentration of MB over 11 h. The degradation efficiency, kinetic rate constant and determination coefficient parameters of the samples are given in Table 2. The k values obtained from the slope of the lines in Fig. 7b show that the most enhanced photocatalytic degradation of MB was obtained with the S3 sample. The photocatalytic degradation of MB was shown to be linked with the anodizing parameters such voltage and time using the k values obtained. As the surface morphology and dimensions of the structure change with changing anodizing parameters, the photocatalytic performance also changes in relation to this. The photocatalytic degradation rate was calculated for all samples using Eq. 10:

$$\ln \frac{C_0}{C} = kt \quad (10)$$

where C₀, C and t are the initial concentration of MB, the concentration of MB at certain time and irradiation time, respectively.

Many factors such as nanostructure, surface area, crystallinity, phase composition, crystal orientation and structure dimensions affect photocatalytic performance. The degradation efficiencies of MB with an initial absorbance value of 0.695 at 664 nm by different samples were calculated for each sample. The results obtained are given in Table 2 and shown as a bar graph in Fig. 8. As can be seen from Fig. 8, the degradation efficiency after 11 h for the arbitration sample is 21.8% while it is 90.6% for the S3 sample.

Fig. 3 SEM micrographs of samples anodized for 30 min at (a) 10 V, (b) 20 V, (c) 30 V, (d) 40 V, and (e) 1000 × magnification of S4 sample



With this degradation efficiency value, the S3 sample has the best photocatalytic performance. It is thought that the reason for the S3 sample having the best photocatalytic activity is that the surface morphology is densely composed of independently formed thin and long NWs. As a result, photocatalysts with different photocatalytic activity values can be obtained by controlling the anodization time and voltage,

which have significant effects on the dimensions of the NWs.

Absorption spectra of MB for sample S3 were drawn for different durations and are shown in Fig. 9a. MB was degraded under UV–Vis light source using S3 sample for 11 h. The absorbance value of MB at 664 nm, which was kept under UV–Vis light illumination for 11 h, has reduced from 0.695 to 0.065

Fig. 4 SEM micrographs of samples anodized at 10 V for (a) 10 min, (b) 20 min, (c) 60 min, and (d) 120 min

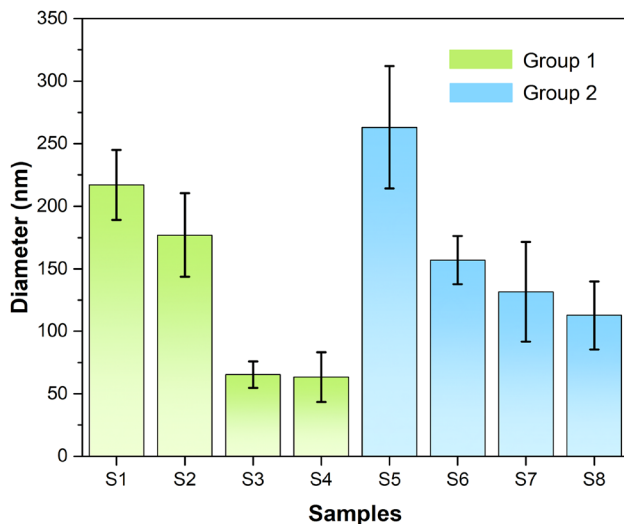
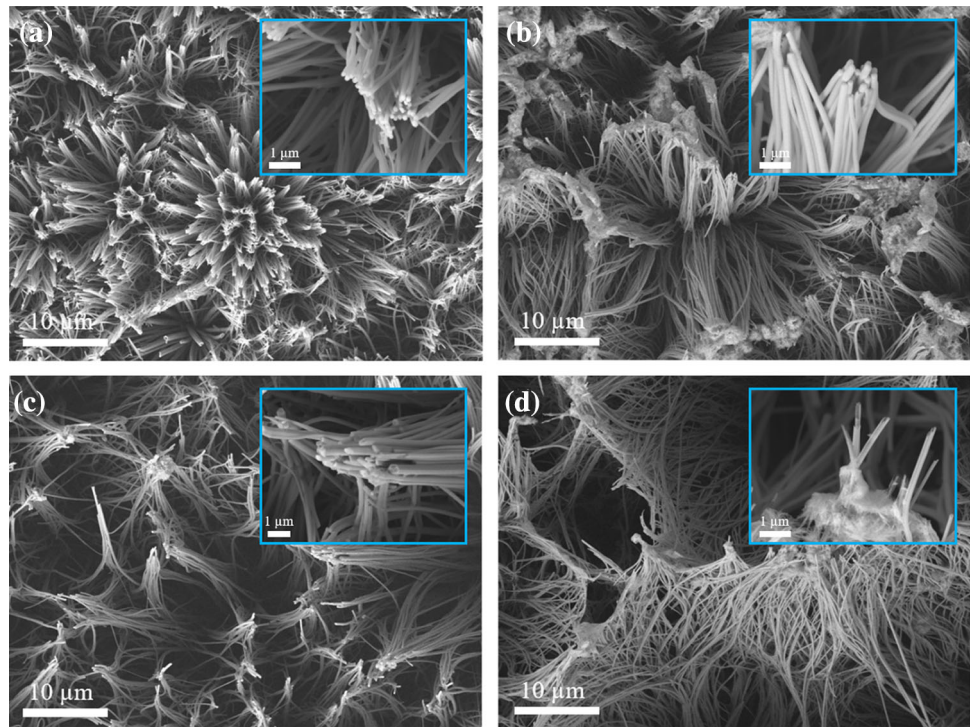


Fig. 5 Diameters of the ZnO NWs

with the degradation efficiency of 90.6% in the presence of the S3 sample.

The stability/reusability test of the samples was performed after 6 months under the same conditions by recording the absorbance values during the

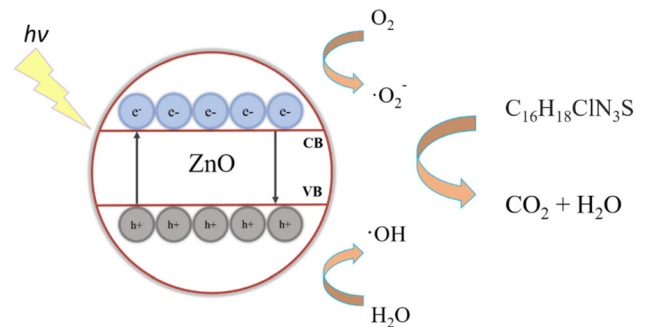


Fig. 6 Photocatalytic degradation mechanism of MB by ZnO structure

degradation of MB by the S3 sample. The absorption spectra were plotted using the obtained data is given in Fig. 9b. According to the results obtained after 6 months, the fact that the S3 sample had almost the same performance showed that there was no change in the structure of the ZnO nanowires produced by the anodizing method. Thus, it has been proven that the S3 sample has high stability and reusability properties.

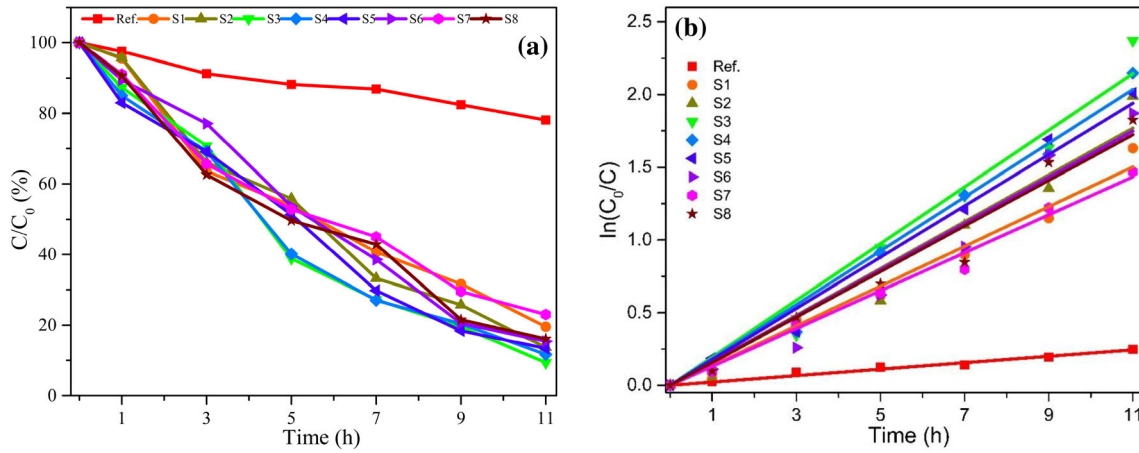


Fig. 7 **a** Photocatalytic degradation of MB solution in the presence of a ZnO NW-structured samples and **b** kinetics of the samples

Table 2 Photocatalytic parameters of the ZnO NW-structured samples

Samples	Ref	Group 1				Group 2			
		S1	S2	S3	S4	S5	S6	S7	S8
Degradation efficiency (%)	21.8	80.4	86.3	90.6	88.3	86.6	84.6	77.9	83.8
Kinetic rate constant (k) (10^{-3} min^{-1})	0.374	2.471	3.015	3.590	3.256	3.047	2.835	2.225	2.765
R^2	0.992	0.992	0.983	0.988	0.994	0.99	0.980	0.996	0.986

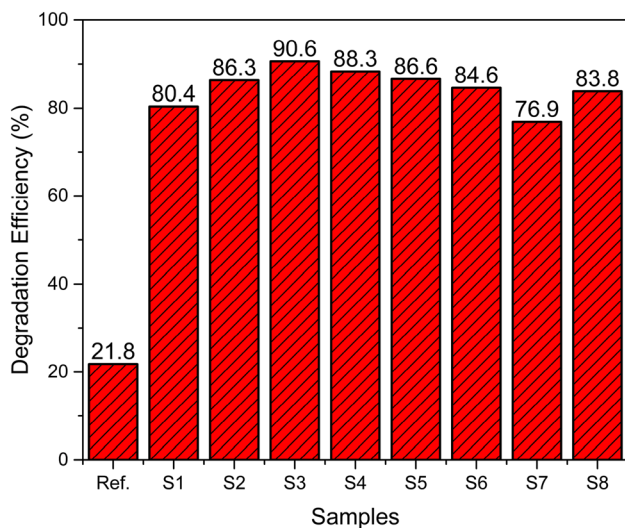


Fig. 8 Photocatalytic degradation efficiencies of the samples after 11 h

4 Conclusion

In summary, ZnO NWs were successfully formed on Zn plates using facile electrochemical anodization method in potassium bicarbonate aqueous electrolytes at different anodizing parameters. The structural characteristics of the ZnO NWs can be controlled by various growth parameters. The obtained SEM results reveal that ZnO NWs have become thinner and denser structures with increasing applied voltage and anodization time. Furthermore, cracking on the surfaces happened at voltages over 30 V. In addition to the structural results the hierarchical ZnO NWs structure has emerged after anodization for 60 min. On the basis of these photocatalysts, the highest photocatalytic efficiency with 90.6% belongs to the sample anodized at 30 V for 30 min. This result shows that NW-structured ZnO

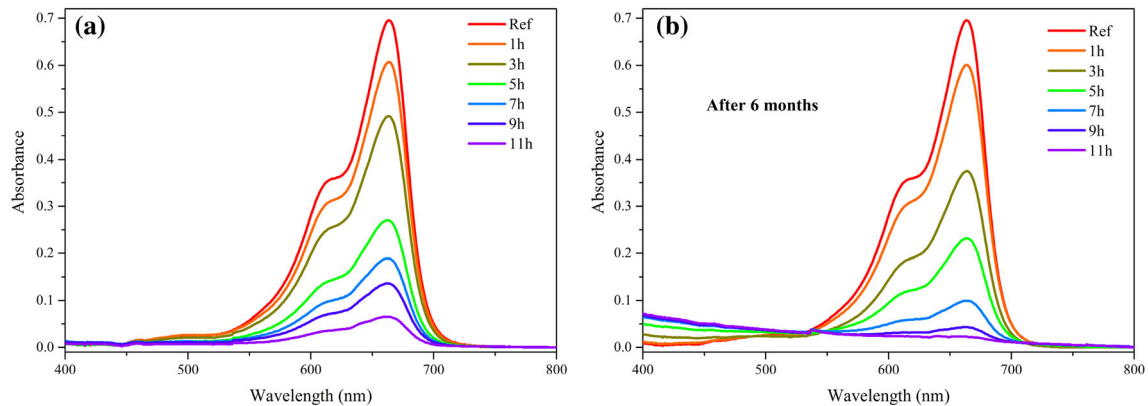


Fig. 9 a UV absorption spectra of MB for S3 sample anodized at 30 V for 30 min, b result of the stability/reusability test of S3 sample after 6 months

materials are promising that they can be used as effective photocatalysts in the conversion of organic pollutants by solar energy into green compounds.

Declarations

Conflict of interest The authors declare that they have no conflict of interest.

References

1. A. Yavaş, S. Güler, M. Erol, Growth of ZnO nanoflowers: effects of anodization time and substrate roughness on structural, morphological, and wetting properties. *J. Aust. Ceram. Soc.* **56**, 995–1003 (2020). <https://doi.org/10.1007/s41779-019-00440-5>
2. M. Erol, T. Dikici, M. Toparli, E. Celik, The effect of anodization parameters on the formation of nanoporous TiO₂ layers and their photocatalytic activities. *J. Alloys Compd.* **604**, 66–72 (2014). <https://doi.org/10.1016/j.jallcom.2014.03.105>
3. D.F. Ollis, Photocatalytic purification and remediation of contaminated air and water. *Compt. Rend. Acad. Des Sci Ser. IIC Chem.* **3**, 405–411 (2000). [https://doi.org/10.1016/S1387-1609\(00\)01169-5](https://doi.org/10.1016/S1387-1609(00)01169-5)
4. R.Y. Hong, J.H. Li, L.L. Chen, D.Q. Liu, H.Z. Li, Y. Zheng, J. Ding, Synthesis, surface modification and photocatalytic property of ZnO nanoparticles. *Powder Technol.* **189**, 426–432 (2009). <https://doi.org/10.1016/j.powtec.2008.07.004>
5. K.M. Lee, C.W. Lai, K.S. Ngai, J.C. Juan, Recent developments of zinc oxide based photocatalyst in water treatment technology: a review. *Water Res.* **88**, 428–448 (2016). <https://doi.org/10.1016/j.watres.2015.09.045>
6. A. Fujishima, X. Zhang, D.A. Tryk, TiO₂ photocatalysis and related surface phenomena. *Surf. Sci. Rep.* **63**, 515–582 (2008). <https://doi.org/10.1016/j.surfrep.2008.10.001>
7. A. Fujishima, K. Honda, Electrochemical photolysis of water at a semiconductor electrode. *Nature* **238**, 37–38 (1972). <https://doi.org/10.1038/238037a0>
8. D.M. Fouad, M.B. Mohamed, Comparative study of the photocatalytic activity of semiconductor nanostructures and their hybrid metal nanocomposites on the photodegradation of malathion. *J. Nanomater.* (2012). <https://doi.org/10.1155/2012/524123>
9. Y.J. Jang, C. Simer, T. Ohm, Comparison of zinc oxide nanoparticles and its nano-crystalline particles on the photocatalytic degradation of methylene blue. *Mater. Res. Bull.* **41**, 67–77 (2006). <https://doi.org/10.1016/j.materresbull.2005.07.038>
10. Z. Hu, Q. Chen, Z. Li, Y. Yu, L.M. Peng, Large-scale and rapid synthesis of ultralong ZnO nanowire films via anodization. *J. Phys. Chem. C.* **114**, 881–889 (2010). <https://doi.org/10.1021/jp9094744>
11. S.E. Ahn, J.L. Soo, H. Kim, S. Kim, B.H. Kang, K.H. Kim, G.T. Kim, Photoresponse of sol-gel-synthesized ZnO nanorods. *Appl. Phys. Lett.* **84**, 5022–5024 (2004). <https://doi.org/10.1063/1.1763633>
12. L. Zaraska, K. Mika, K. Syrek, G.D. Sulka, Formation of ZnO nanowires during anodic oxidation of zinc in bicarbonate electrolytes. *J. Electroanal. Chem.* **801**, 511–520 (2017). <https://doi.org/10.1016/j.jelechem.2017.08.035>
13. J. Dong, Z. Liu, J. Dong, D. Ariyanti, Z. Niu, S. Huang, W. Zhang, W. Gao, Self-organized ZnO nanorods prepared by anodization of zinc in NaOH electrolyte. *RSC Adv.* **6**, 72968–72974 (2016). <https://doi.org/10.1039/c6ra16995c>
14. C. Tian, Q. Zhang, A. Wu, M. Jiang, B. Jiang, H. Fu, Cost-effective large-scale synthesis of ZnO photocatalyst with excellent performance for dye photodegradation. *Chem.*

- Commun. **48**, 2858–2860 (2012). <https://doi.org/10.1039/c2cc16434e>
15. R. Kumar, A. Umar, G. Kumar, H.S. Nalwa, A. Kumar, M.S. Akhtar, Zinc oxide nanostructure-based dye-sensitized solar cells. *J. Mater. Sci.* **52**, 4743–4795 (2017). <https://doi.org/10.1007/s10853-016-0668-z>
 16. A. Achour, M.A. Soussou, K. Ait Aissa, M. Islam, N. Barreau, E. Faulques, L. Le Brizoual, M.A. Djouadi, M. Boujita, Nanostructuring and band gap emission enhancement of ZnO film via electrochemical anodization. *Thin Solid Films* **571**, 168–174 (2014). <https://doi.org/10.1016/j.tsf.2014.10.061>
 17. N. Tiwale, Zinc oxide nanowire gas sensors: fabrication, functionalisation and devices. *Mater. Sci. Technol.* (United Kingdom) **31**, 1681–1697 (2015). <https://doi.org/10.1179/1743284714Y.0000000747>
 18. Y. Zhang, M.K. Ram, E.K. Stefanakos, D.Y. Goswami, Synthesis, characterization, and applications of ZnO nanowires. *J. Nanomater.* (2012). <https://doi.org/10.1155/2012/624520>
 19. A. Mateen Tantray, M.A. Shah, Photo electrochemical ability of dense and aligned ZnO nanowire arrays fabricated through electrochemical anodization. *Chem. Phys. Lett.* **747**, 137346 (2020). <https://doi.org/10.1016/j.cplett.2020.137346>
 20. J.Y. Kim, J.W. Cho, S.H. Kim, The characteristic of the ZnO nanowire morphology grown by the hydrothermal method on various surface-treated seed layers. *Mater. Lett.* **65**, 1161–1164 (2011). <https://doi.org/10.1016/j.matlet.2010.10.092>
 21. J.L. Yang, S.J. An, W. Il Park, G.C. Yi, W. Choi, Photocatalysis using ZnO thin films and nanoneedles grown by metal-organic chemical vapor deposition. *Adv. Mater.* **16**, 1661–1664 (2004). <https://doi.org/10.1002/adma.200306673>
 22. Y.H. Chen, Y.M. Shen, S.C. Wang, J.L. Huang, Fabrication of one-dimensional ZnO nanotube and nanowire arrays with an anodic alumina oxide template via electrochemical deposition. *Thin Solid Films* **570**, 303–309 (2014). <https://doi.org/10.1016/j.tsf.2014.03.014>
 23. A. Menzel, K. Subannajui, R. Bakhda, Y. Wang, R. Thomann, M. Zacharias, Tuning the growth mechanism of ZnO nanowires by controlled carrier and reaction gas modulation in thermal CVD. *J. Phys. Chem. Lett.* **3**, 2815–2821 (2012). <https://doi.org/10.1021/jz301103s>
 24. K. Subannajui, F. Güder, J. Danhof, A. Menzel, Y. Yang, L. Kirste, C. Wang, V. Cimalla, U. Schwarz, M. Zacharias, An advanced fabrication method of highly ordered ZnO nanowire arrays on silicon substrates by atomic layer deposition. *Nanotechnology* **23**, 7 (2012). <https://doi.org/10.1088/0957-4484/23/23/235607>
 25. C. Florica, N. Preda, A. Costas, I. Zgura, I. Enculescu, ZnO nanowires grown directly on zinc foils by thermal oxidation in air: Wetting and water adhesion properties. *Mater. Lett.* **170**, 156–159 (2016). <https://doi.org/10.1016/j.matlet.2016.02.035>
 26. J. Huang, H. Ren, P. Sun, C. Gu, Y. Sun, J. Liu, Facile synthesis of porous ZnO nanowires consisting of ordered nanocrystallites and their enhanced gas-sensing property. *Sens. Actuat. B Chem.* **188**, 249–256 (2013). <https://doi.org/10.1016/j.snb.2013.06.103>
 27. P. Batista-Grau, R. Sánchez-Tovar, R.M. Fernández-Domene, J. García-Antón, Formation of ZnO nanowires by anodization under hydrodynamic conditions for photoelectrochemical water splitting. *Surf. Coatings Technol.* **381**, 125197 (2020). <https://doi.org/10.1016/j.surfcoat.2019.125197>
 28. A. Ramirez-Canon, D.O. Miles, P.J. Cameron, D. Mattia, Zinc oxide nanostructured films produced via anodization: a rational design approach. *RSC Adv.* **3**, 25323–25330 (2013). <https://doi.org/10.1039/c3ra43886d>
 29. H. Masuda, K. Fukuda, Ordered metal nanohole arrays made by a two-step replication of honeycomb structures of anodic alumina. *Science (80-)* **268**, 1466–1468 (1995). <https://doi.org/10.1126/science.268.5216.1466>
 30. D.O. Miles, P.J. Cameron, D. Mattia, Hierarchical 3D ZnO nanowire structures via fast anodization of zinc. *J. Mater. Chem. A.* **3**, 17569–17577 (2015). <https://doi.org/10.1039/c5ta03578c>
 31. A. Ramirez-canon, D.O. Miles, J. Cameron, D. Mattia, Zinc oxide nanostructured films via anodization: a rational design approach. *RSC Adv.* **3**(47), 25323–25330 (2013). <https://doi.org/10.1039/c3ra43886d>
 32. L. Zaraska, K. Mika, M. Zych, G.D. Sulka, Anodic formation of zinc oxide nanostructures with various morphologies. *INC* (2020). <https://doi.org/10.1016/b978-0-12-816706-9.00012-1>
 33. P. Batista-Grau, R.M. Fernández-Domene, R. Sánchez-Tovar, J. García-Antón, Control on the morphology and photoelectrocatalytic properties of ZnO nanostructures by simple anodization varying electrolyte composition. *J. Electroanal. Chem.* **880**, 114933 (2021). <https://doi.org/10.1016/J.JELECHEM.2020.114933>
 34. Y.T. Kim, J. Park, S. Kim, D.W. Park, J. Choi, Fabrication of hierarchical ZnO nanostructures for dye-sensitized solar cells. *Electrochim. Acta.* **78**, 417–421 (2012). <https://doi.org/10.1016/j.electacta.2012.06.022>
 35. A. Ramirez-Canon, M. Medina-Llamas, M. Vezzoli, D. Mattia, Multiscale design of ZnO nanostructured photocatalysts. *Phys. Chem. Chem. Phys.* **20**, 6648–6656 (2018). <https://doi.org/10.1039/c7cp07984b>
 36. M.U. Anu Prathap, B. Kaur, R. Srivastava, Hydrothermal synthesis of CuO micro-/nanostructures and their applications

- in the oxidative degradation of methylene blue and non-enzymatic sensing of glucose/H₂O₂. *J. Colloid Interface Sci.* **370**, 144–154 (2012). <https://doi.org/10.1016/j.jcis.2011.12.074>
37. S. Demirci, T. Dikici, M. Yurddaskal, S. Gultekin, M. Toparli, E. Celik, Synthesis and characterization of Ag doped TiO₂ heterojunction films and their photocatalytic performances. *Appl. Surf. Sci.* **390**, 591–601 (2016). <https://doi.org/10.1016/j.apsusc.2016.08.145>
38. Y. Zhang, J. Zhou, X. Chen, Q. Feng, W. Cai, MOF-derived C-doped ZnO composites for enhanced photocatalytic performance under visible light. *J. Alloys Compd.* **777**, 109–118 (2019). <https://doi.org/10.1016/J.JALLCOM.2018.10.383>
39. R. Selvaraj, K.R. Kalimuthu, V. Kalimuthu, A type-II MoS₂/ZnO heterostructure with enhanced photocatalytic activity. *Mater. Lett.* **243**, 183–186 (2019). <https://doi.org/10.1016/J.MATLET.2019.02.022>
40. S.S. Lo, T. Mirkovic, C.-H. Chuang, C. Burda, G.D. Scholes, Emergent Properties resulting from type-II band alignment in semiconductor nanoheterostructures. *Adv. Mater.* **23**, 180–197 (2011). <https://doi.org/10.1002/ADMA.201002290>
41. Y. Qu, X. Xu, R. Huang, W. Qi, R. Su, Z. He, Enhanced photocatalytic degradation of antibiotics in water over functionalized N, S-doped carbon quantum dots embedded ZnO nanoflowers under sunlight irradiation. *Chem. Eng. J.* **382**, 123016 (2020). <https://doi.org/10.1016/J.CEJ.2019.123016>
42. P. Nandi, D. Das, ZnO-CuxO heterostructure photocatalyst for efficient dye degradation. *J. Phys. Chem. Solids.* **143**, 109463 (2020). <https://doi.org/10.1016/J.JPCS.2020.109463>
43. S. Kapatel, C.K. Sumesh, Two-step facile preparation of MoS₂/ZnO nanocomposite as efficient photocatalyst for methylene blue (dye) degradation. *Electron. Mater. Lett.* (2018). <https://doi.org/10.1007/s13391-018-00101-y>
44. Y. Lin, R. Hong, H. Chen, D. Zhang, J. Xu, Green synthesis of ZnO-GO composites for the photocatalytic degradation of methylene blue. *J. Nanomater.* (2020). <https://doi.org/10.1155/2020/4147357>

Publisher's Note Springer Nature remains neutral with regard to jurisdictional claims in published maps and institutional affiliations.